Neuron
Article

The Excitatory Neuronal Network of the C2 Barrel Column in Mouse Primary Somatosensory Cortex

Sandrine Lefort,[1] Christian Tomm,[2] J.-C. Floyd Sarria,[3] and Carl C.H. Petersen[1,*]
[1]Laboratory of Sensory Processing, Brain Mind Institute
[2]Laboratory of Computational Neuroscience, Brain Mind Institute
[3]BioImaging and Optics Platform
Faculty of Life Sciences, Ecole Polytechnique Federale de Lausanne (EPFL), CH1015, Switzerland
*Correspondence: carl.petersen@epfl.ch
DOI 10.1016/j.neuron.2008.12.020

SUMMARY

Local microcircuits within neocortical columns form key determinants of sensory processing. Here, we investigate the excitatory synaptic neuronal network of an anatomically defined cortical column, the C2 barrel column of mouse primary somatosensory cortex. This cortical column is known to process tactile information related to the C2 whisker. Through multiple simultaneous whole-cell recordings, we quantify connectivity maps between individual excitatory neurons located across all cortical layers of the C2 barrel column. Synaptic connectivity depended strongly upon somatic laminar location of both presynaptic and postsynaptic neurons, providing definitive evidence for layer-specific signaling pathways. The strongest excitatory influence upon the cortical column was provided by presynaptic layer 4 neurons. In all layers we found rare large-amplitude synaptic connections, which are likely to contribute strongly to reliable information processing. Our data set provides the first functional description of the excitatory synaptic wiring diagram of a physiologically relevant and anatomically well-defined cortical column at single-cell resolution.

INTRODUCTION

The sophisticated information processing power of the mammalian brain is thought to derive in large part from computations in synaptically connected neocortical neuronal networks. Anatomical data demonstrate that the vast majority of synapses in the neocortex are formed between nearby neurons, with long-range axonal projections making smaller contributions (Braitenberg and Schüz, 1998; Douglas et al., 1995). Such so-called "small-world networks" with dense local connectivity and sparse long-range interactions are considered to be highly efficient in reducing wiring length while allowing rapid and complex information processing (Watts and Strogatz, 1998).

Normal to its surface, the neocortex is characterized by vertically arranged columns divided into layers containing different types of neurons. Neocortical areas differ in organization and are specialized for processing different types of information. Primary sensory areas are organized in highly ordered maps tangential to the cortical surface with nearby regions processing closely related sensory information. One of the most remarkable cortical maps is found in the rodent primary somatosensory cortex, where each whisker is represented in layer 4 (L4) by an anatomically defined unit, termed a "barrel" (Woolsey and Van der Loos, 1970). A cortical "barrel column" can be defined as the vertical thickness of the neocortex laterally bounded by the width of the L4 barrel. Among cortical areas explored in different species, the barrel cortex is unique in offering a precise anatomical definition for a cortical column with clear functional correlates in the underlying synaptic circuits (Bureau et al., 2004, 2006; Feldmeyer et al., 1999, 2002; Petersen and Sakmann, 2000, 2001; Schubert et al., 2001, 2003, 2006; Shepherd et al., 2003, 2005; Shepherd and Svoboda, 2005; Silver et al., 2003). Tactile sensory information is processed somatotopically within the barrel map, such that deflection of a single whisker initially evokes cortical neuronal activity within its related barrel column (recently reviewed by Petersen, 2007). In order to understand how information is processed in this cortical microcircuit, it will be essential to quantify the underlying synaptic connectivity of the individual neurons.

Electrophysiological recordings in brain slices currently provide the highest-resolution technique for analyzing functional synaptic interactions between individual neocortical neurons (Silberberg et al., 2005; Thomson and Lamy, 2007). Dual whole-cell recordings in the rat barrel cortex have already provided detailed information about synaptic transmission between specific types of excitatory neurons (Feldmeyer et al., 1999, 2002, 2005, 2006; Petersen and Sakmann, 2000; Brasier and Feldman, 2008; Frick et al., 2008), but an overall analysis of excitatory synaptic connectivity within an entire cortical column has not yet been attempted. Here, through multiple simultaneous in vitro whole-cell recordings, we specifically and quantitatively investigated the excitatory synaptic circuits of the mouse C2 barrel column.

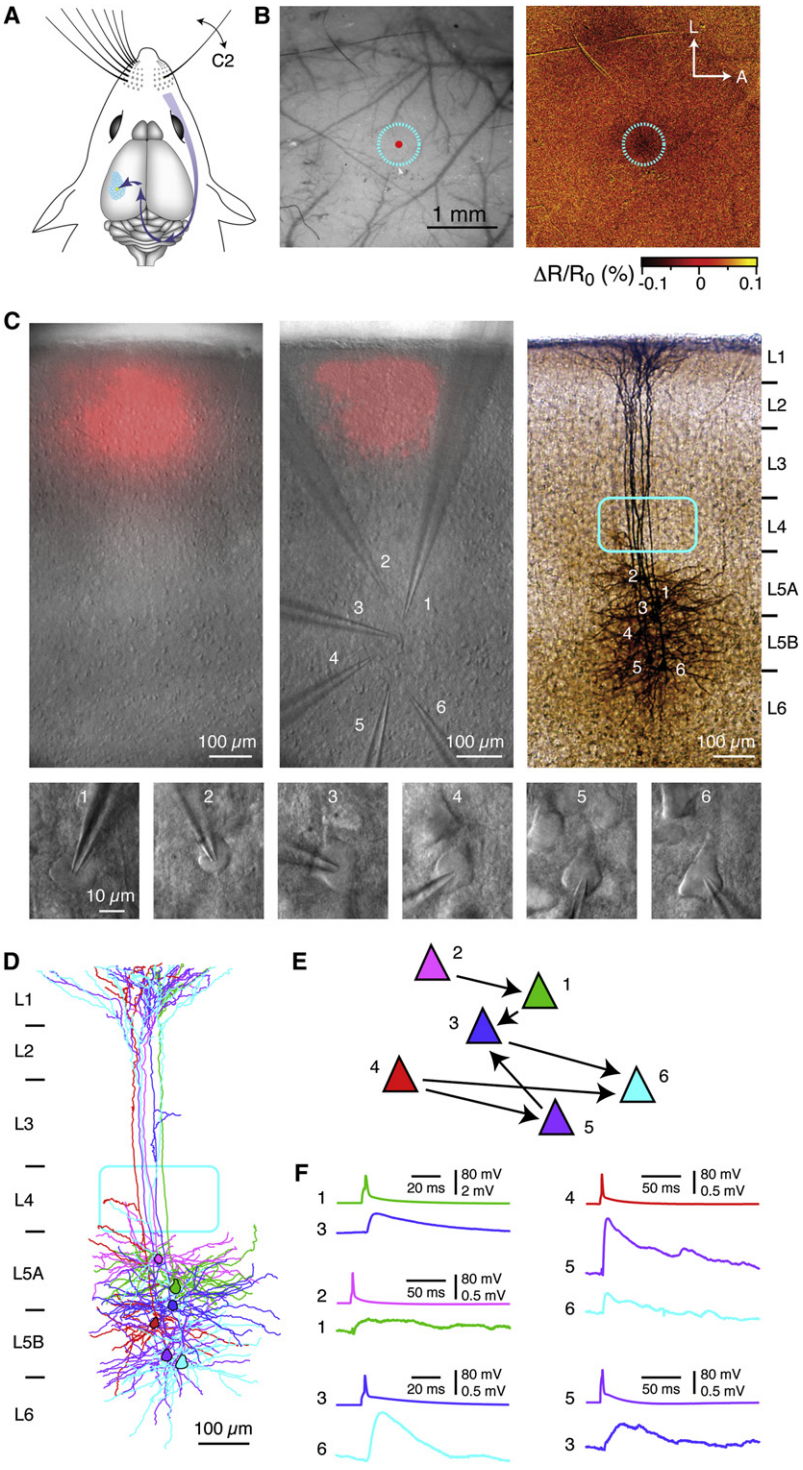

Figure 1. Whole-Cell Recordings Targeted In Vitro to the Mouse C2 Barrel Column

(A) Deflection of the C2 whisker evokes activity in the C2 barrel column of primary somatosensory cortex.

(B) Intrinsic optical imaging shows a decreased reflectance (right; L indicates lateral, A indicates anterior) localizing the C2 barrel column relative to the surface blood vessels (left).

(C) Fluorescent dye (SR101) applied to the C2 barrel column after intrinsic optical imaging can be found in brain slices in vitro (left). Infrared gradient contrast optics are used to target whole-cell recordings to neurons located in the C2 barrel column (middle and lower panels). During recordings the neurons are filled with biocytin, which allows post hoc identification of neuronal structure (right).

(D) Color-coded dendritic reconstructions of the recorded neurons.

(E) Color-coded schematic synaptic connectivity diagram.

(F) Color-coded membrane potential traces showing presynaptic action potentials (APs) and unitary excitatory postsynaptic potentials (uEPSPs) in the synaptically connected neurons.

RESULTS

Targeting In Vitro Whole-Cell Recordings to the Mouse C2 Barrel Column

In order to specifically target our microcircuit analysis to the C2 barrel column, each experiment began with intrinsic optical imaging (Grinvald et al., 1986) to functionally locate the C2 whisker representation (Ferezou et al., 2006). Under urethane anesthesia, the C2 whisker was repeatedly deflected at 10 Hz for 4 s, which evoked a highly localized hemodynamic response at the location of the C2 barrel column (Figures 1A and 1B). Through alignment of the functional imaging with the surface blood vessels, fluorescent dye was applied to specifically label the C2 barrel column. Parasagittal slices were subsequently prepared with an angle of 35° away from vertical, which was found to be the optimal angle for keeping intact the axonal and dendritic arborizations of neurons in the C2 barrel column. We next screened the brain slices and, in general, only one or two slices were labeled with the fluorescent dye. The brain slice with the brightest fluorescence, locating the C2 barrel column, was selected for electrophysiological recordings (Figure 1C). The somata of individual neurons of the C2 barrel column were visualized using infrared gradient contrast video microscopy. Simultaneous somatic whole-cell recordings were obtained from two to six neurons, allowing investigation of the electrical properties of the neurons and an evaluation of their synaptic connectivity. In the example experiment (Figures 1C–1F), we recorded simultaneously from six pyramidal neurons. By injecting a brief 2 ms depolarizing current pulse, we evoked an action potential (AP) in each of these neurons in turn, while recording the membrane potential of the other neurons. For synaptically coupled excitatory neurons, a presynaptic AP evokes release of glutamate, which opens postsynaptic ionotropic glutamate receptors, resulting in a unitary excitatory postsynaptic potential (uEPSP) measured at the

soma. For every presynaptic neuron in a microcircuit containing 6 neurons, there are 5 possible target cells, giving a total of 30 possible synaptic connections. In this example experiment we found 6 synaptic connections out of the possible 30, giving a synaptic connection probability of 20%.

Synaptic connectivity differed from experiment to experiment and so, in order to obtain quantitative information, it is clearly important to record from many pairs of neurons. Altogether in this study, we recorded from a total of 2550 neurons specifically located in the mouse C2 barrel column across 322 slices from 307 mice (in a few experiments we recorded from neurons in the C2 barrel column of 2 adjacent slices, both containing bright fluorescent labeling). We tested 8895 possible synaptic connections and we found 909 functional synaptic connections, giving a value of 10.2% as the overall observed connectivity. However, synaptic connectivity was not uniform, but rather depended strongly upon the somatic laminar location of the recorded neurons within the C2 barrel column.

Excitatory Neurons of the Mouse C2 Barrel Column

We assigned neocortical layer boundaries (Figure 2A) based on both high-contrast micrographs obtained during the electrophysiological experiments (Figure 1C) and post hoc DAPI fluorescence showing locations of cell nuclei (Figures 2B and 2C). DAPI staining was carried out in fixed slices after every experiment together with the staining procedures to reveal the morphology of the recorded neurons. Across 313 slices, we found the following subpial distances (mean ± SEM) for the lower boundaries of the different layers: L1, 128 ± 1 μm; L2, 269 ± 2 μm; L3, 418 ± 3 μm; L4, 588 ± 3 μm; L5A, 708 ± 4 μm; L5B, 890 ± 5 μm; L6, 1154 ± 7 μm.

In agreement with previous studies, we found different types of excitatory neurons in different cortical layers (Figure 2A). In L3, L5A, and L5B, we recorded exclusively from pyramidal neurons with a prominent apical dendrite oriented toward the pia. In L2, we additionally recorded from modified pyramidal neurons, in which the apical dendrite was less obvious or horizontally oriented. In L4, most neurons were spiny stellate neurons (82%) with a small fraction of star pyramidal neurons (18%). Most recorded pyramidal neurons in L5A had small tufts in L1 (89%), whereas the apical dendrite of many L5B pyramids bifurcated in L3/4 and had an extensive tuft in L1 (71%). In L6, we recorded from short pyramidal neurons (94%) and inverted pyramidal neurons (6%). Resting membrane potential (V_m), input resistance (R_{in}), membrane time-constants (Tau), AP threshold, AP amplitude, and rheobase varied across layers (Table 1).

To quantify the number of excitatory neurons in different layers of the mouse C2 barrel column, we stained slices with a NeuN antibody to specifically visualize the location of neuronal somata combined with DAPI to locate all nuclei. In order to separately label GABAergic neurons in these anatomical experiments, we used knockin mice expressing GFP from the GAD67 gene locus (Tamamaki et al., 2003) (Figures 2B and 2C). NeuN-positive cells lacking GFP labeling were considered as excitatory neurons. We made 3D confocal stacks of 100 μm thick sections of the C2 barrel column for six mice. The number and locations of neuronal somata were found by an automated spot detection algorithm followed by manual correction and verification. The C2 barrel column is ~300 μm in diameter, and as a first-order approximation for the total number of excitatory neurons in this column, we multiplied the cell counts obtained from the 100 μm thick sections by a factor of three. Our estimates for the mean ± SEM number of excitatory neurons in each layer are as follows: L2, 546 ± 49; L3, 1145 ± 132; L4, 1656 ± 83; L5A, 454 ± 46; L5B, 641 ± 50; L6, 1288 ± 84 (Figure 2D). We estimate the following numbers of GABAergic neurons in different layers of the mouse C2 barrel column (mean ± SEM): L1, 26 ± 8; L2, 107 ± 7; L3, 123 ± 19; L4, 140 ± 9; L5A, 90 ± 14; L5B, 131 ± 6; L6, 127 ± 9 (Figure 2D).

Excitatory Synaptic Circuits of the Mouse C2 Barrel Column

We next analyzed the synaptic connectivity with respect to the laminar locations of the somata of both presynaptic and postsynaptic neurons. The most prominent excitatory synaptic circuit in the mouse C2 barrel column is formed between neurons within a single L4 barrel (Feldmeyer et al., 1999; Petersen and Sakmann, 2000). In an example experiment (Figure 3A), three spiny stellate neurons were recorded in L4 and large uEPSPs were evoked at each of the six possible L4→L4 synaptic connections in this microcircuit. In this example experiment, we also recorded from two L3 pyramidal neurons and further L4→L3 and L3→L3 synaptic connections were identified. In another example experiment (Figure 3B), the two neurons in L4 were not synaptically coupled, but both provided synaptic input to a neuron in L5A. In this experiment, three L5A neurons were recorded and three synaptic connections were found among these L5A neurons.

Altogether within L4, we found 254 excitatory synaptic connections among 1046 tested connections, giving an average probability of any two excitatory L4 neurons being synaptically connected as 24.3% (which we will denote as $P_{L4\rightarrow L4}$ = 24.3%). The peak L4→L4 uEPSP amplitudes ranged from 0.06 mV to 7.79 mV (mean ± SEM = 0.95 ± 0.08 mV; median = 0.52 mV) (Table 2). We also quantified the uEPSP kinetics (see Table S1 and Figure S1 available online). Among these synaptically connected pairs of neurons, we found that 59 were reciprocally bidirectionally connected. This is close to the value of 62 reciprocal connections expected for a randomly wired network (given by 24.3% × 24.3% × 1046) (Table S2). However, in other respects the neocortical excitatory synaptic pathways appear far from randomly organized. For example, we found evidence for highly specific patterns of connectivity between L4 and the other layers. Excitatory output from L4 to all other cortical layers is substantial, with over 10% connectivity for L4→L2, L4→L3, and L4→L5A ($P_{L4\rightarrow L2}$ = 12%, $P_{L4\rightarrow L3}$ = 14.5%, and $P_{L4\rightarrow L5A}$ = 11.6%). The mean output connectivity from L4 to other layers is 10.8%. In contrast, it receives very little input from the other cortical layers, with the strongest input to L4 originating from L3 with $P_{L3\rightarrow L4}$ = 2.4% and the mean interlaminar input connectivity to L4 being 1.0% (Figure 3C; Table 2).

Tactile information relating to single whisker deflections is in part signaled via thalamocortical neurons of the ventral posterior medial nucleus (VPM) providing important input to L4 neurons. With their strong output connectivity to other cortical layers,

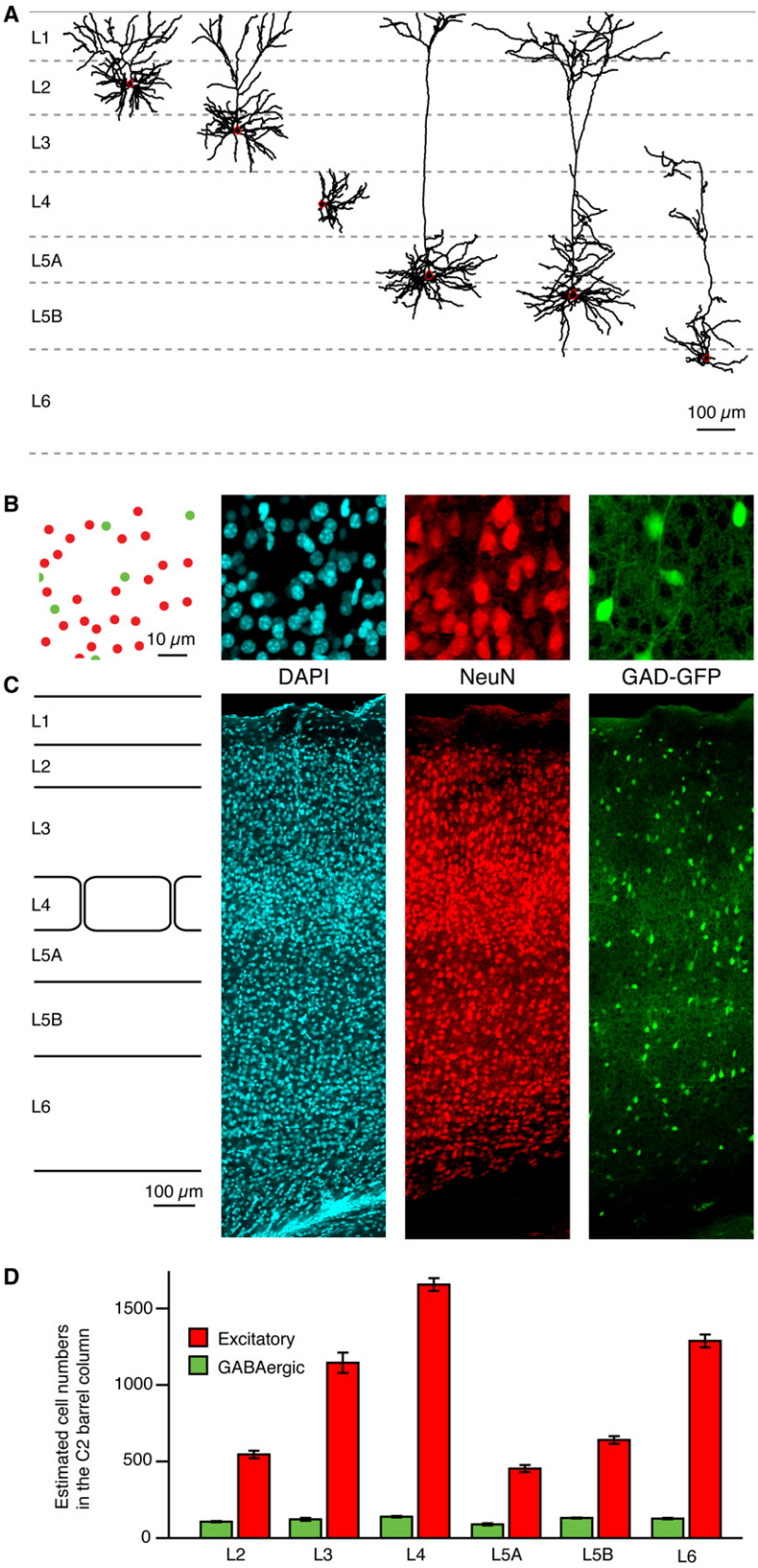

Figure 2. Excitatory Neurons of the Mouse C2 Barrel Column

(A) Examples of different dendritic morphologies found in the mouse C2 barrel column. Layer boundaries are drawn to scale at their mean subpial distance.

(B) Confocal images of DAPI-stained nuclei (cyan), NeuN-stained neurons (red), and GFP expressed in GABAergic neurons (green) of a GAD67-GFP knockin mouse. Red dots indicate location of excitatory neurons; green dots, GABAergic neurons (left).

(C) Confocal image of a single focal plane through the C2 barrel column, stained as above.

(D) Estimated numbers (mean ± SEM) of excitatory and inhibitory cells in different layers of the mouse C2 barrel column.

Table 1. Intrinsic Electrophysiological Properties of Excitatory Neurons in the Mouse C2 Barrel Column

	L2	L3	L4	L5A	L5B	L6
Resting V_m (mV)	−72.0 ± 0.3	−71.4 ± 0.4	−66.0 ± 0.3	−62.8 ± 0.2	−63.0 ± 0.3	−66.8 ± 0.4
R_{in} (MΩ)	188 ± 3	193 ± 5	302 ± 4	210 ± 3	162 ± 5	277 ± 4
Tau (ms)	28.3 ± 0.3	30.0 ± 0.6	34.8 ± 0.5	37.6 ± 0.6	25.8 ± 0.7	28.2 ± 0.5
AP threshold (mV)	−38.3 ± 0.2	−38.7 ± 0.2	−39.7 ± 0.2	−38.9 ± 0.2	−41.1 ± 0.2	−40.2 ± 0.3
AP amplitude from threshold to peak (mV)	72.4 ± 0.4	73.5 ± 0.5	70.9 ± 0.4	70.2 ± 0.5	73.1 ± 0.5	69.9 ± 0.5
Rheobase (pA)	126 ± 3	132 ± 4	56 ± 1	68 ± 2	98 ± 3	76 ± 3

Values are mean ± SEM. Statistically significant differences ($p < 0.05$) were assessed by performing a nonparametric Kruskal-Wallis test followed by a post hoc Dunn-Holland-Wolfe test for pairwise comparison. Statistically significant differences were found for the following: Resting V_m: L2 versus L4, L2 versus L5A, L2 versus L5B, L2 versus L6, L3 versus L4, L3 versus L5A, L3 versus L5B, L3 versus L6, L4 versus L5A, L4 versus L5B, L5A versus L6, and L5B versus L6. R_{in}: L2 versus L4, L2 versus L5A, L2 versus L5B, L2 versus L6, L3 versus L4, L3 versus L5A, L3 versus L5B, L3 versus L6, L4 versus L5A, L4 versus L5B, L5A versus L5B, L5A versus L6, and L5B versus L6. Tau: L2 versus L4, L2 versus L5A, L2 versus L5B, L3 versus L4, L3 versus L5A, L3 versus L5B, L4 versus L5B, L4 versus L6, L5A versus L5B, L5A versus L6, and L5B versus L6. AP threshold: L2 versus L4, L2 versus L5B, L2 versus L6, L3 versus L4, L3 versus L5B, L3 versus L6, L4 versus L5A, L4 versus L5B, L4 versus L6, L5A versus L5B, and L5A versus L6. AP amplitude: L2 versus L5A, L2 versus L6, L3 versus L4, L3 versus L5A, L3 versus L6, L4 versus L5B, L5A versus L5B, and L5B versus L6. Rheobase: L2 versus L4, L2 versus L5A, L2 versus L5B, L2 versus L6, L3 versus L4, L3 versus L5A, L3 versus L5B, L3 versus L6, L4 versus L5A, L4 versus L5B, L4 versus L6, L5A versus L5B, and L5B versus L6.

the excitatory neurons of L4 are in a good position to distribute this sensory information to both supragranular and infragranular cortical layers within the C2 barrel column.

Both supragranular and infragranular layers are also highly synaptically connected. Connectivity is remarkably high in L3 ($P_{L3\rightarrow L3}$ = 18.7%) and L5A ($P_{L5A\rightarrow L5A}$ = 19.1%), but lower in L2 ($P_{L2\rightarrow L2}$ = 9.3%), L5B ($P_{L5B\rightarrow L5B}$ = 7.2%), and L6 ($P_{L6\rightarrow L6}$ = 2.8%). In supragranular layers, we found that pathways toward the more superficial layers dominate: $P_{L4\rightarrow L3}$ = 14.5% versus $P_{L3\rightarrow L4}$ = 2.4% (χ^2 test, $p = 5.3 \times 10^{-5}$); $P_{L4\rightarrow L2}$ = 12% versus $P_{L2\rightarrow L4}$ = 0.96% (χ^2 test, $p = 4.7 \times 10^{-6}$); $P_{L3\rightarrow L2}$ = 12.1% versus $P_{L2\rightarrow L3}$ = 5.5% (χ^2 test, p = 0.03) (Figure S2). Conversely, in infragranular layers, pathways toward deeper layers dominate: $P_{L4\rightarrow L5A}$ = 11.6% versus $P_{L5A\rightarrow L4}$ = 0.7% (χ^2 test, $p = 1.2 \times 10^{-7}$); $P_{L4\rightarrow L5B}$ = 8.1% versus $P_{L5B\rightarrow L4}$ = 0.7% (χ^2 test, p = 0.003); $P_{L5A\rightarrow L5B}$ = 8% versus $P_{L5B\rightarrow L5A}$ = 1.7% (χ^2 test, p = 0.006).

We also examined the excitatory synaptic networks directly linking supragranular and infragranular layers. In two example experiments (Figures 4A and 4B), we illustrate two of the most important excitatory pathways from supragranular to infragranular layers (L2→L5A and L3→L5B). There was a clear overall directionality favoring excitation from supragranular to infragranular layers: $P_{L2\rightarrow L5A}$ = 9.5% versus $P_{L5A\rightarrow L2}$ = 4.3% (χ^2 test, p = 0.037); $P_{L2\rightarrow L5B}$ = 8.3% versus $P_{L5B\rightarrow L2}$ = 0.96% (χ^2 test, p = 0.011); $P_{L3\rightarrow L5A}$ = 5.7% versus $P_{L5A\rightarrow L3}$ = 2.2% (χ^2 test, p = 0.23); $P_{L3\rightarrow L5B}$ = 12.2% versus $P_{L5B\rightarrow L3}$ = 1.8% (χ^2 test, $p = 1.9 \times 10^{-4}$) (Figures 4C–4F). Finally, we found sparse connectivity with L6 neurons, with a mean probability of finding a synaptically connected cell in any layer with an L6 neuron being 3.0%. The only major input to L6 came from L5B ($P_{L5B\rightarrow L6}$ = 7%). No important outputs from L6 to other layers were identified in the C2 barrel column.

Synaptic Connectivity Matrices for the Mouse C2 Barrel Column

The overall summary of the layer-specific excitatory synaptic connectivity can be conveniently represented in the form of a numerical (Table 2) or a color-coded matrix (Figure 5A). In addition to the probability of finding connected pairs of neurons between presynaptic and postsynaptic neurons in specific layers, the efficacy of the identified connections can be assessed through quantifying the peak uEPSP amplitude. In excitatory pathways where we found five or more synaptic connections, the layer-specific uEPSP amplitude (mean ± SEM) ranged from 0.22 ± 0.04 mV (L2→L5B) to 1.01 ± 0.24 mV (L3→L5B) (Figure 5B; Table 2). However, as discussed below, these differences did not reach significance due to the large range of uEPSP amplitudes found within each type of layer-specific synaptic connection. The average layer-specific excitatory impact of a single AP in a presynaptic neuron can be computed as the product of the probability of finding the given synaptic connection and its mean uEPSP amplitude (Figure 5C). This product quantifies the mean uEPSP amplitude evoked in the average neuron of a specific layer, if a single neuron located in a given layer is stimulated to evoke a single AP. Qualitatively, this product matrix follows a similar pattern of connectivity to that described by the connection probabilities.

Finally, in order to avoid any potential bias introduced by classifying neurons into layers, we also computed the same synaptic connectivity matrices based on the subpial distance of the somata of both the presynaptic and postsynaptic neurons with 50 μm spatial binning (Figures 5D–5F). These unbiased connectivity matrices are in excellent agreement with the layer-classified matrices (Figures 5A–5C). In addition, these spatial connectivity matrices of the C2 barrel column microcircuit indicate further specificity. Within L2, as defined through DAPI staining (Figure S3A), the upper 50 μm appears to receive substantially more input from L5A (and also to provide more input to L5A) than the lower part of L2 (Figure S3B), in agreement with previous work (Bureau et al., 2006). In future studies, it might even be useful to define neocortical layers based on functional connectivity maps. We also analyzed horizontal connectivity within our data set and, in agreement with a previous report (Song et al., 2005), we found no significant

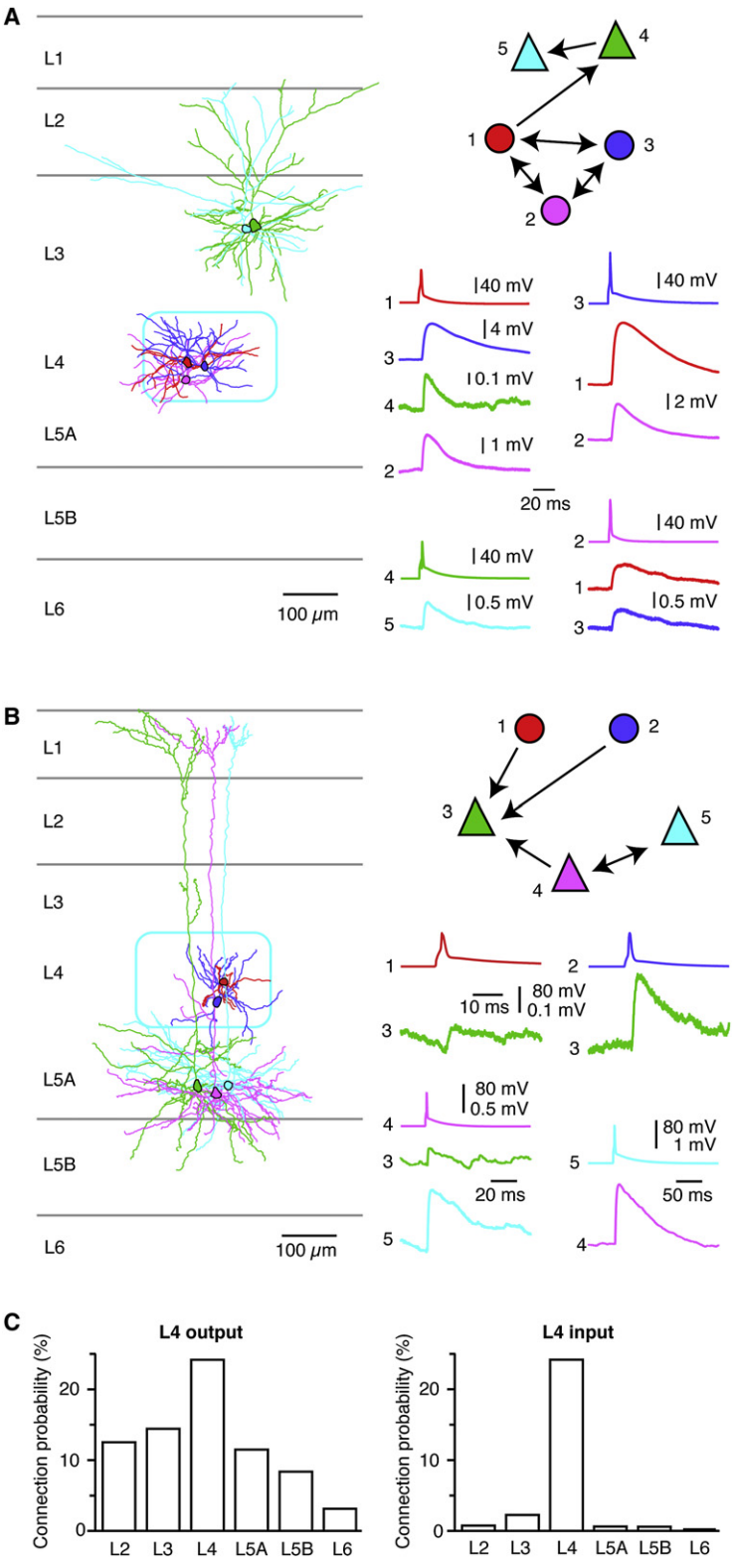

Figure 3. Layer 4 Neurons Provide Strong Excitatory Output to the C2 Barrel Column, but They Receive Little Input from Other Layers

(A) Example experiment showing synaptic connectivity in a small microcircuit containing three spiny stellate L4 neurons and two pyramidal neurons in L3.

(B) A different example experiment analyzing connectivity between L4 and L5A.

(C) Averaged across many experiments, we find high connectivity from L4 to other layers (left), but very little input to L4 from other layers (right).

drop in connectivity over the small horizontal distances explored in the current study of the mouse C2 barrel column (Figure S4).

Distributions of uEPSP Amplitudes and Reliability

The uEPSP amplitude connectivity matrices shown in Figure 5B indicate the layer-specific mean uEPSP connection amplitudes. However, within the data set for each layer-specific connection we found a very large range of individual uEPSP amplitudes across different synaptically connected pairs of neurons (Table 2). Across the entire data set, the mean amplitudes of synaptic connections were distributed over more than two orders of magnitude, ranging from 0.04 mV to 7.79 mV (mean ± SEM = 0.75 ± 0.03 mV; median = 0.43 mV). An example experiment (Figures 6A and 6B) shows a divergent connection, with an AP in a single L4 presynaptic neuron evoking both a large reliable uEPSP in another L4 neuron (Figure 6A) and also a smaller highly variable uEPSP in an L3 neuron (Figure 6B). In general, we found few large-amplitude synaptic connections but many small synaptic connections, giving rise to a highly skewed distribution of uEPSP amplitudes (Brunel et al., 2004; Feldmeyer et al., 1999, 2002, 2006; Frick et al., 2008; Song et al., 2005) (Figure 6C). Such uEPSP amplitude distributions with a long tail formed by rare large-amplitude uEPSPs were found in all layers (Figure S5). The skewed distribution is also indicated by the median uEPSP amplitude being smaller than the mean for 21 out of the 24 excitatory pathways where we found 3 or more synaptic connections (Table 2).

The trial-to-trial variability of large-amplitude uEPSPs is very low (Figure 6A) compared with the highly variable responses found at small-amplitude synaptic connections (Figure 6B). This striking relationship can be quantified by plotting the coefficient of variation (Table S3) as a function of uEPSP amplitude (Feldmeyer et al., 1999, 2002, 2006; Frick et al., 2008) (Figure 6D). The increased reliability of large-amplitude uEPSPs, quantified as a reduction in the coefficient of variation, was found in all cortical layers (Figure S6).

Although rare, these large-amplitude reliable synaptic connections could dominate the entire network activity through convergent synaptic circuits forming functional neuronal assemblies.

Table 2. Excitatory Synaptic Connectivity and uEPSP Amplitudes in the Mouse C2 Barrel Column

		Presynaptic					
Postsynaptic		L2	L3	L4	L5A	L5B	L6
L2	P (found/tested)	9.3% (88/950)	12.1% (22/182)	12.0% (25/208)	4.3% (9/209)	0.96% (1/104)	0% (0/50)
	mean ± SEM	0.64 ± 0.06 mV	0.71 ± 0.15 mV	0.98 ± 0.24 mV	0.52 ± 0.13 mV	0.21 mV	
	median	0.46 mV	0.59 mV	0.58 mV	0.52 mV		
	range	0.08 – 3.88 mV	0.04 – 2.67 mV	0.07 – 5.54 mV	0.08 – 1.09 mV		
L3	P (found/tested)	5.5% (10/183)	18.7% (96/513)	14.5% (25/172)	2.2% (2/89)	1.8% (3/167)	0% (0/64)
	mean ± SEM	0.44 ± 0.09 mV	0.78 ± 0.07 mV	0.58 ± 0.13 mV	0.67 mV	0.26 ± 0.08 mV	
	median	0.35 mV	0.48 mV	0.35 mV		0.32 mV	
	range	0.09 – 1.02 mV	0.08 – 2.76 mV	0.07 – 3.33 mV	0.15 – 1.19 mV	0.10 – 0.35 mV	
L4	P (found/tested)	0.96% (2/208)	2.4% (4/170)	24.3% (254/1046)	0.7% (2/275)	0.7% (1/137)	0% (0/94)
	mean ± SEM	0.31 mV	0.36 ± 0.09 mV	0.95 ± 0.08 mV	0.48 mV	0.17 mV	
	median		0.31 mV	0.52 mV			
	range	0.18 – 0.45 mV	0.22 – 0.61 mV	0.06 – 7.79 mV	0.22 – 0.74 mV		
L5A	P (found/tested)	9.5% (20/211)	5.7% (5/87)	11.6% (32/276)	19.1% (178/934)	1.7% (3/174)	0.6% (1/160)
	mean ± SEM	0.55 ± 0.10 mV	0.93 ± 0.26 mV	0.54 ± 0.09 mV	0.66 ± 0.06 mV	0.24 ± 0.09 mV	0.08 mV
	median	0.40 mV	1.09 mV	0.38 mV	0.37 mV	0.19 mV	
	range	0.08 – 2.03 mV	0.08 – 1.54 mV	0.06 – 1.98 mV	0.05 – 5.24 mV	0.11 – 0.41 mV	
L5B	P (found/tested)	8.3% (9/108)	12.2% (20/164)	8.1% (11/136)	8.0% (14/175)	7.2% (40/555)	2% (2/100)
	mean ± SEM	0.22 ± 0.04 mV	1.01 ± 0.24 mV	0.88 ± 0.25 mV	0.88 ± 0.36 mV	0.71 ± 0.19 mV	0.30 mV
	median	0.20 mV	0.51 mV	0.44 mV	0.60 mV	0.29 mV	
	range	0.09 – 0.47 mV	0.06 – 4.05 mV	0.07 – 2.61 mV	0.13 – 5.45 mV	0.08 – 7.16 mV	0.12 – 0.48 mV
L6	P (found/tested)	0% (0/50)	0% (0/61)	3.2% (3/93)	3.2% (5/158)	7.0% (7/100)	2.8% (15/532)
	mean ± SEM			2.27 ± 1.72 mV	0.28 ± 0.09 mV	0.49 ± 0.16 mV	0.53 ± 0.19 mV
	median			0.96 mV	0.27 mV	0.43 mV	0.26 mV
	range			0.17 – 5.67 mV	0.06 – 0.58 mV	0.14 – 1.36 mV	0.09 – 3.00 mV

The probability of finding a synaptically connected pair of neurons with somata of presynaptic and postsynaptic neurons located in the specific layers is denoted by "P." The number of functional synaptic connections identified is indicated by "found," whereas the number of pairs recorded (both connected and unconnected) is indicated by "tested." The peak uEPSP amplitudes in terms of the layer-specific mean ± SEM, median, and range are quantified in mV. No significant differences were found comparing uEPSP amplitudes. According to a χ^2 statistic on contingency table, significant differences (χ^2 test $p < 0.05$) in connectivity were found for L2→L2 versus L2→L4, L2→L2 versus L3→L3, L2→L2 versus L4→L4, L2→L2 versus L5A→L4, L2→L2 versus L5A→L5A, L2→L2 versus L6→L6, L2→L3 versus L3→L3, L2→L3 versus L4→L4, L2→L3 versus L5A→L5A, L2→L4 versus L3→L2, L2→L4 versus L3→L3, L2→L4 versus L3→L5B, L2→L4 versus L4→L2, L2→L4 versus L4→L3, L2→L4 versus L4→L4, L2→L4 versus L4→L5A, L2→L4 versus L5A→L5A, L2→L5A versus L4→L4, L2→L5A versus L5A→L4, L2→L5B versus L5A→L4, L2→L6 versus L4→L4, L3→L2 versus L5A→L4, L3→L2 versus L6→L5A, L3→L2 versus L6→L6, L3→L3 versus L3→L4, L3→L3 versus L5A→L2, L3→L3 versus L5A→L4, L3→L3 versus L5A→L6, L3→L3 versus L5B→L2, L3→L3 versus L5B→L3, L3→L3 versus L5B→L4, L3→L3 versus L5B→L5A, L3→L3 versus L5B→L5B, L3→L3 versus L6→L4, L3→L3 versus L6→L5A, L3→L3 versus L6→L5B, L3→L3 versus L6→L6, L3→L4 versus L4→L3, L3→L4 versus L4→L4, L3→L4 versus L5A→L5A, L3→L5A versus L4→L4, L3→L5B versus L5A→L4, L3→L5B versus L6→L5A, L3→L5B versus L6→L6, L3→L6 versus L4→L4, L4→L2 versus L5A→L4, L4→L2 versus L6→L5A, L4→L2 versus L6→L6, L4→L3 versus L5A→L4, L4→L3 versus L5B→L3, L4→L3 versus L5B→L4, L4→L3 versus L5B→L5A, L4→L3 versus L6→L5A, L4→L3 versus L6→L6, L4→L4 versus L4→L5A, L4→L4 versus L4→L5B, L4→L4 versus L4→L6, L4→L4 versus L5A→L2, L4→L4 versus L5A→L3, L4→L4 versus L5A→L4, L4→L4 versus L5A→L5B, L4→L4 versus L5A→L6, L4→L4 versus L5B→L2, L4→L4 versus L5B→L3, L4→L4 versus L5B→L4, L4→L4 versus L5B→L5A, L4→L4 versus L5B→L5B, L4→L4 versus L6→L2, L4→L4 versus L6→L3, L4→L4 versus L6→L4, L4→L4 versus L6→L5A, L4→L4 versus L6→L5B, L4→L4 versus L6→L6, L4→L5A versus L5A→L4, L4→L5A versus L6→L5A, L4→L5A versus L6→L6, L4→L5B versus L5A→L4, L5A→L2 versus L5A→L5A, L5A→L3 versus L5A→L5A, L5A→L4 versus L5A→L5A, L5A→L4 versus L5A→L5B, L5A→L4 versus L5B→L5B, L5A→L5A versus L5A→L6, L5A→L5A versus L5B→L2, L5A→L5A versus L5B→L3, L5A→L5A versus L5B→L4, L5A→L5A versus L5B→L5A, L5A→L5A versus L5B→L5B, L5A→L5A versus L6→L4, L5A→L5A versus L6→L5A, L5A→L5A versus L6→L5B, and L5A→L5A versus L6→L6.

We tested this hypothesis through computational network modeling.

Visualization of the C2 Neuronal Network

The experimental data quantifying the numbers of excitatory neurons in different layers, their intrinsic electrophysiological properties, and their synaptic connectivity can be used to construct simple integrate-and-fire computer simulations (Gerstner and Kistler, 2002) of the neuronal network of the C2 barrel column (Figures 7A–7C). In order to visualize the relative impact of activity in different layers, we graphically plotted the color-coded peak membrane potential changes of each neuron evoked

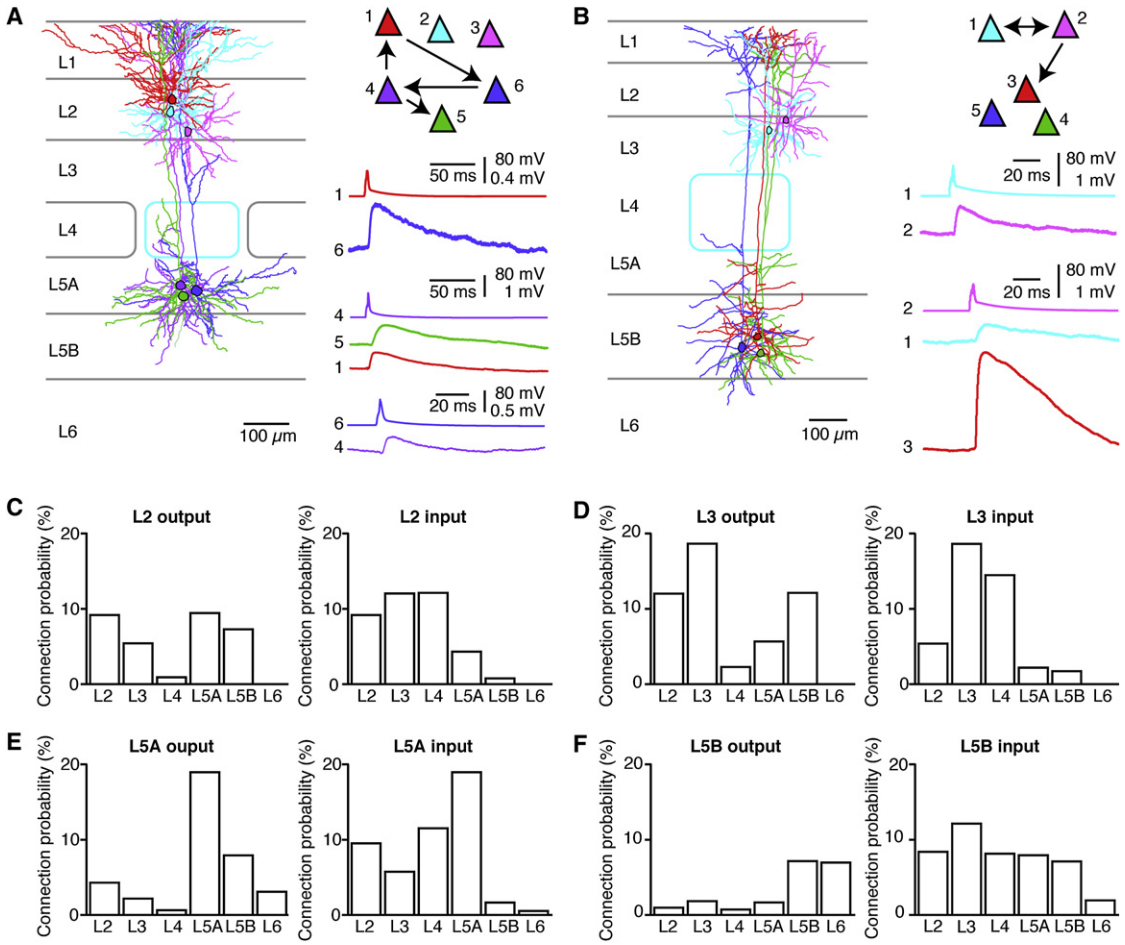

Figure 4. Excitatory Synaptic Networks Linking Supragranular and Infragranular Layers

(A) Example experiment analyzing synaptic connectivity between L2 and L5A. (B) Example experiment analyzing synaptic connectivity between L3 and L5B. (C–F) The layer-specific mean input and output connectivity from L2 (C), L3 (D), L5A (E), and L5B (F).

by stimulating a single AP in one randomly chosen neuron in a given layer in the computer simulation (Figure 7A). These visualizations clearly indicate the sparseness of strong synaptic connections, which are highlighted through the chosen color scale.

Assuming linear summation of uEPSPs, we also visualized the effect of simultaneously evoking an AP in ten randomly selected neurons in the same layer (Figure 7B). In these images the connectivity patterns described in the mean connection matrices (Figures 5A–5C) become evident. For example the synchronous excitation of ten neurons in L2 evokes the most obvious responses in L2 and L5A; activity in L3 evokes prominent responses in L2, L3, and L5B; and excitation of L4 evokes activity throughout the column. Stimulation of L5A neurons evokes responses in L5A and L5B together with L2 and L3; L5B evokes activity in L5B and L6. Such simulations therefore provide a simple and direct way to visualize the relative layer-specific impacts of activity within the C2 barrel column and offer a step toward understanding the excitatory pathways for information processing within a cortical column.

Rare Large-Amplitude uEPSPs May Contribute Substantially to Network Activity

We next used our integrate-and-fire simulation of the C2 neuronal network to quantitatively examine the effect of the rare large-amplitude synaptic connections on network activity. We compared three different neuronal networks. The first network (the same one as used above; here termed the "experiment network") was wired according to the experimentally observed uEPSP distribution. A second network was similarly wired except that the amplitude of each synaptic connection between specific layers was set to the layer-specific mean (termed the "mean network"). Finally, a third network (termed the "big uEPSP network") was wired according to the experimentally observed uEPSP distribution, except that every connection below a strength of 500 μV was removed from the network. This resulted in an overall reduction in the total number of synaptic connections to less than half of the real connectivity.

We computed the minimal number of synchronously active presynaptic neurons, each firing a single AP, that are required to drive further spikes in an otherwise quiescent network wired

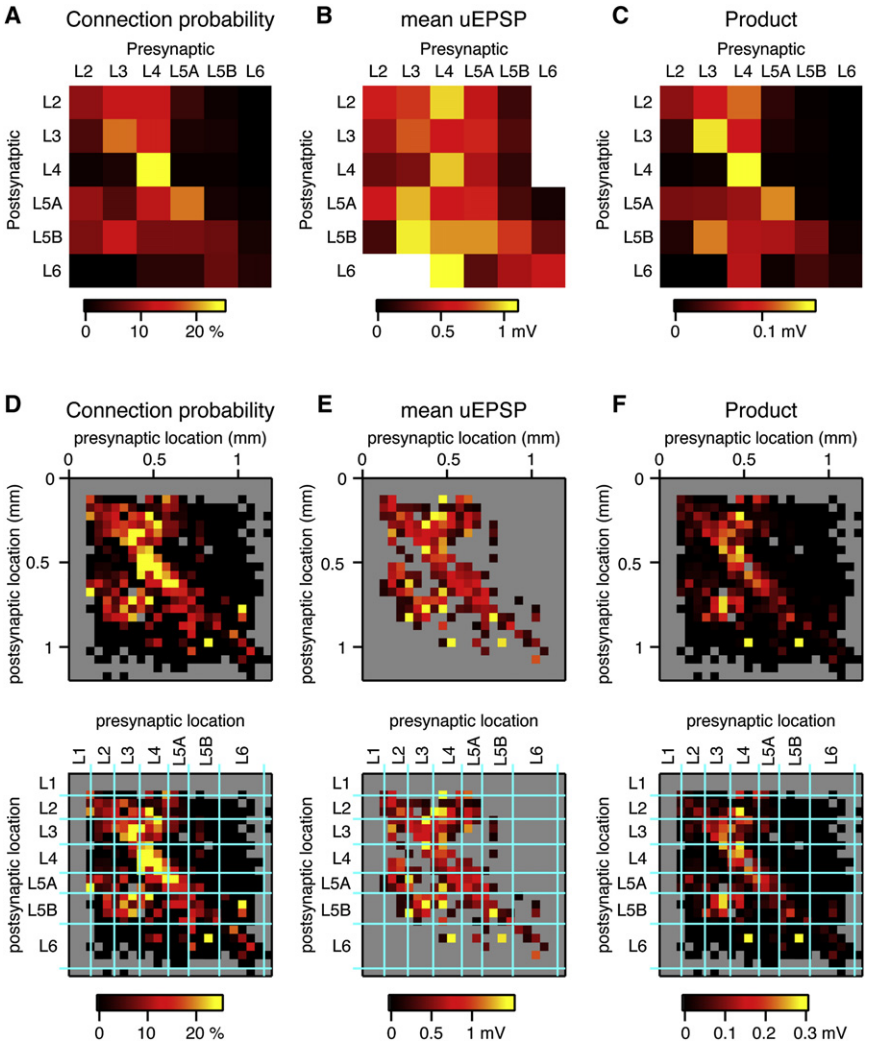

Figure 5. Connectivity Matrices for the Mouse C2 Barrel Column

(A) Color-coded matrix showing the probability of finding a connected pair of neurons between specific layers.

(B) The equivalent matrix showing the mean uEPSP amplitude of synaptic connections between specific layers.

(C) The product of the probability of finding a synaptic connection and its amplitude provides an estimate of mean layer-specific impact of a single AP in a given layer of the C2 cortical column.

(D) The probability of finding synaptically connected pairs of neurons based on the subpial somatic location of the presynaptic and postsynaptic neurons binned at 50 μm intervals. The lower panel displays the same data, but with the mean locations of layer boundaries superimposed in cyan.

(E) The uEPSP amplitude of synaptically coupled pairs of neurons based on the subpial somatic location of the presynaptic and postsynaptic neurons binned at 50 μm intervals.

(F) The product of the synaptic connection probability and the uEPSP amplitude based on the subpial somatic location of the presynaptic and postsynaptic neurons binned at 50 μm intervals.

assuming linear summation. The smallest number was found in L4, which required only 30 ± 6 neurons (mean ± SD, Figure 7D) to be stimulated in the experiment network. However, twice this number of L4 neurons (64 ± 4 neurons, mean ± SD) needed to be stimulated in the mean network. The most important difference between the mean network and the experiment network is the presence of the rare large-amplitude uEPSPs in the experiment network. This motivated us to compare the big uEPSP network to the experiment network. Strikingly, we found that the removal of more than half of the weaker synaptic connections had little effect on the threshold number of L4 neurons (31 ± 6 neurons, mean ± SD) for evoking further APs. These results demonstrate that the few large uEPSPs of the experiment network make strong contributions to network excitability, resulting from the chance convergence of rare large-amplitude uEPSP connections onto postsynaptic target neurons, which are therefore driven to spike.

We carried out the same threshold quantification for all layers in our neuronal network simulation. For each layer, we computed the ratio of the threshold number of neurons required to evoke further APs in the reduced networks (mean network or big uEPSP network) compared to the number of neurons needing to be stimulated in networks with the synaptic connectivity of the full experimental data set (experiment network) (Figure 7E). Large threshold ratios comparing the mean network and the experiment network were obtained for L3, L4, and L5A, indicating a prominent role for the long-tailed uEPSP amplitude distribution. The threshold ratios close to unity for L3, L4, L5A, L5B, and L6 comparing the big uEPSP network to the experiment network directly indicate that the large-amplitude uEPSPs dominate network activity, even though they only represent a minority of all the synaptic connections.

DISCUSSION

Through multiple simultaneous whole-cell recordings targeted by intrinsic optical imaging to the mouse C2 barrel column, we have made the first attempt to characterize and quantify the excitatory synaptic circuits within a well-defined cortical column at single-cell resolution in a genetically tractable model animal. These data provide the beginnings of a framework for analyzing the functional operation of the cortical circuits in the mouse C2 barrel column. In future studies it will be of interest to use this quantitative data to constrain the analysis of membrane potential dynamics recorded in pyramidal neurons of the C2 barrel column of awake mice (Crochet and Petersen, 2006; Poulet and

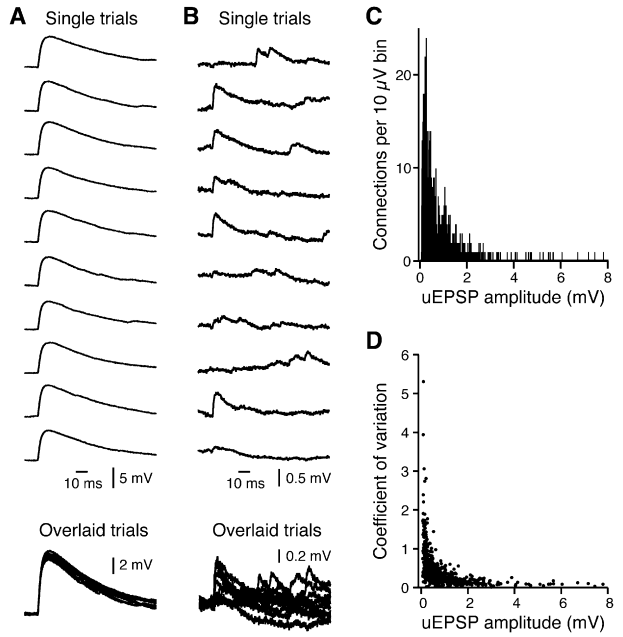

Figure 6. The Rare Large-Amplitude uEPSPs May Contribute Importantly to Network Activity

(A) Ten individual trials from a large-amplitude synaptic connection showing little trial-to-trial variability. The presynaptic neuron was located in L4 and corresponds to cell 1 in Figure 3A. The postsynaptic neuron was also in L4 and corresponds to cell 3 in Figure 3A.

(B) The same presynaptic L4 neuron (cell 1 in Figure 3A) made a divergent connection to an L3 pyramid (cell 4 in Figure 3A) with a small-amplitude uEPSP, which exhibited substantial trial-to-trial variability.

(C) The distribution of the mean uEPSP synaptic connection amplitudes found across the entire data set, binned at 10 μV intervals. Note the long tail, indicating rare large-amplitude synaptic connections.

(D) The distribution of the coefficient of variation quantified across the entire data set and plotted as a function of the mean uEPSP amplitude of each synaptic connection found in this study.

Petersen, 2008), a process that has already been begun for the analysis of sensory processing in the anesthetized rat barrel cortex (Sarid et al., 2007).

The impact of an individual cortical column upon behavior is not currently known. However, the "gap-crossing" task can be carried out by single-whisker animals and depends upon an intact barrel cortex (Hutson and Masterton, 1986; Harris et al., 1999). It is therefore clear that even a single whisker can provide sufficient information for decision making. Studying the synaptic connectivity and functional operation of a single cortical column may therefore provide useful information relating to sensory perception.

Layer-Specific Pathways for Excitatory Signal Flow in the Mouse C2 Barrel Column

We found layer-specific interlaminar and intralaminar microcircuits within a cortical column. The synaptic connectivity matrices (Figure 5) lack symmetry along the main diagonal, revealing the prominence of direction-specific synaptic interactions. Our data provide strong evidence supporting the existence of specific excitatory pathways for information flow within a cortical column, which are likely to be determined through a combination of genetically defined programs and activity-dependent synaptic plasticity.

The product of the probability of finding a given synaptic connection and its mean uEPSP amplitude is the simplest way to quantify its importance. Thresholding at 0.1 mV reveals the five most significant synaptic connections in the C2 barrel column: L3→L3, L4→L4, L5A→L5A, L4→L2, and L3→L5B (Figure 8A). The most important upward-oriented synaptic connections thresholded at a product value of 0.05 mV are L3→L2, L4→L2, and L4→L3 (Figure 8B). There are many more downward-oriented synaptic connections with a product value over this 0.05 mV threshold: L2→L5A, L3→L5A, L3→L5B, L4→L5A, L4→L5B, L4→L6, and L5A→L5B (Figure 8C).

These synaptic pathways, which we quantified in mouse C2 barrel cortex, are in qualitative agreement with the proposed "canonical" microcircuits of visual cortex (Binzegger et al., 2004) derived from anatomical overlap of axonal and dendritic arborizations, which often provides a good estimate of functional connectivity (Shepherd et al., 2005), as mapped by glutamate uncaging (Callaway and Katz, 1993). However, the circuits we describe differ from the mouse motor cortex (Weiler et al., 2008), which is the only other cortical area that has been functionally studied to an equal degree of completeness including all cortical layers (although not at the resolution of single presynaptic neurons). In motor cortex, the pathway from L2/3 to L5 dominates all other synaptic pathways (Weiler et al., 2008), whereas in barrel cortex, L4 dominates the cortical column. In future studies, it will be of great interest to quantitatively compare differences in microcircuits from different cortical areas.

Functional Operation of the C2 Microcircuit

We know very little about neuronal activity in the cortex of awake, behaving mice. Whole-cell recordings from pyramidal neurons in the supragranular layers of the C2 barrel column of head-fixed mice have revealed large-amplitude spontaneous subthreshold activity generated internally within the central nervous system (Crochet and Petersen, 2006; Poulet and Petersen, 2008), which might relate to top-down input enhancing the saliency of specific neuronal assemblies (Petersen, 2007; Gilbert and Sigman, 2007).

In addition, these neurons respond robustly to whisker-object contacts (Ferezou et al., 2006, 2007; Crochet and Petersen, 2006). Strong feedforward sensory input originating from a single whisker is rapidly signaled to its homologous cortical barrel column via two synapses, one in the brainstem and the other in the thalamus. Thalamocortical input for processing single-whisker information arrives, in part, via the VPM, which projects strongly to L4. The prominent intracortical excitatory synaptic circuits from L4 to all other layers in the cortical column are therefore likely to distribute information relating to the immediately ongoing sensory input to the entire cortical column.

Despite the large-amplitude subthreshold membrane potential fluctuations found in recordings from awake mice, AP firing is infrequent in L2/3 pyramidal neurons of the C2 barrel column (Crochet and Petersen, 2006; Poulet and Petersen, 2008). Sparse AP coding may therefore be relevant in the rodent neocortex (Brecht et al., 2004; Lee et al., 2006; Houweling and Brecht, 2008; Huber et al., 2008; Greenberg et al., 2008). In

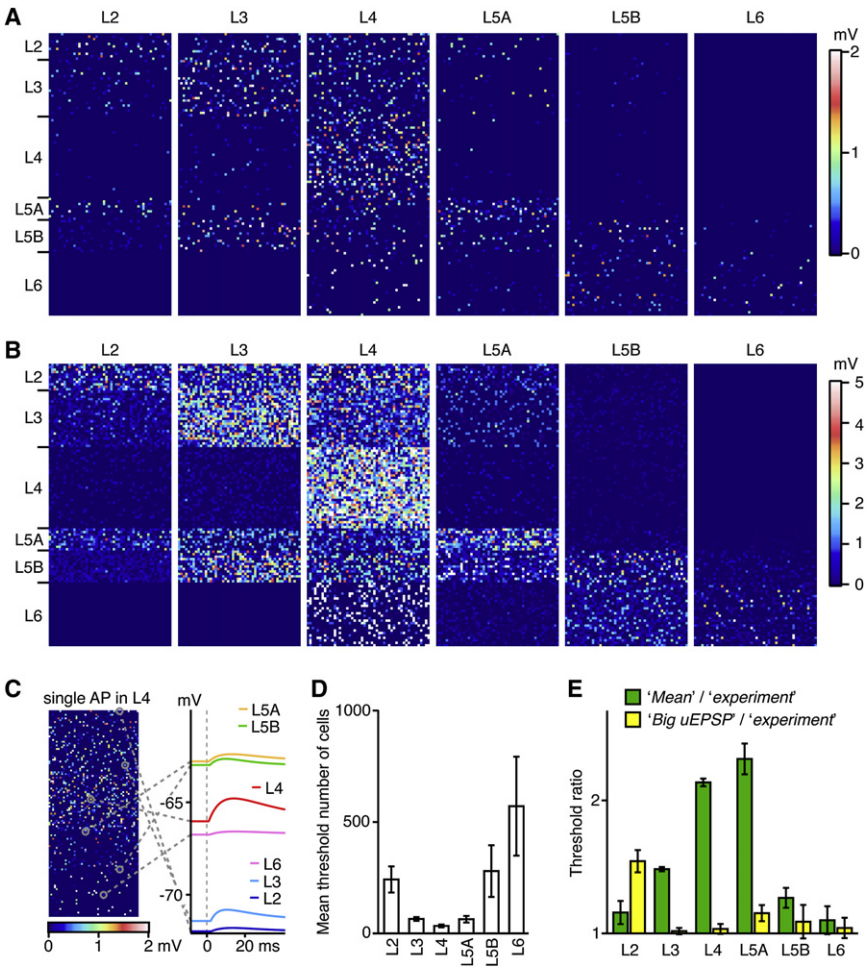

Figure 7. Simulation and Visualization of the Excitatory C2 Neuronal Network

(A) A single AP was evoked in a single randomly chosen neuron of a specific layer (noted above each image) of a simulated C2 barrel column wired following the experimentally observed distribution of uEPSPs. Each neuron is represented as a pixel, color-coded according to the peak amplitude of the synaptically evoked change in membrane potential. Because connectivity is sparse, most neurons do not receive any uEPSP.

(B) As above, but now ten randomly chosen neurons in the same specified layer (noted above each image) are synchronously activated, each firing a single AP.

(C) A single randomly selected neuron in L4 was stimulated and its impact upon the C2 network was visualized as above (left). The membrane potential dynamics of one randomly selected postsynaptic neuron from each layer are shown (right).

(D) In a simulated neuronal network wired according to the experimentally observed uEPSP distribution ("experiment network"), we plot the number (mean ± SD) of synchronously activated neurons in a given layer necessary to evoke further APs in the network.

(E) The ratio (mean ± SEM) of the thresholds for evoking further APs in the mean network compared to the experiment network (green) and the same threshold ratio comparing the big uEPSP network to the experiment network (yellow). The mean network lacks the rare large uEPSP connections of the experiment network. In L3, L4, and L5A, considerably more neurons are needed to be stimulated to evoke network activity in the mean network as compared with the experiment network. The big uEPSP network only considers large uEPSP connections (above 500 μV), and the ratios close to unity for L3, L4, L5A, L5B, and L6 indicate that large synaptic connections drive most network activity.

this context it is interesting to note that our network simulations indicate that synchronous APs in a few neurons of the C2 barrel column may be sufficient to propagate neuronal activity. The convergence of a few low-variance and large-amplitude uEPSP inputs onto target neurons appears to form a key determinant for reliable sparse AP coding. In addition, such sparse network dynamics mediated by rare large-amplitude uEPSPs are compatible with observations in the barrel cortex of awake, behaving mice, indicating that brief, large, and specific synaptic inputs drive spikes in one neuron, while the membrane potential of neighboring neurons remains unaffected without significant depolarization (Poulet and Petersen, 2008).

The rare large-amplitude uEPSPs could therefore link neurons into strongly connected functional cell assemblies (Figure 8D). The strengthening of synapses through correlated activity in presynaptic and postsynaptic neurons (Hebb, 1949; Markram et al., 1997; Feldman, 2000; Sjöström et al., 2001, 2003) is likely to contribute to the formation of these large synaptic connections. The many unreliable small-amplitude uEPSPs might primarily offer neuronal networks opportunities for synaptic plasticity.

Future Perspectives

The intricate synaptic microcircuits of the C2 barrel column interact strongly with many important extrinsic inputs (for example: nearby cortical columns; more distant cortical areas such as secondary somatosensory cortex and motor cortex; and thalamic nuclei). In the future, it will therefore be of critical importance to extend quantitative synaptic network analysis to include entire sensorimotor loops and the actions of neuromodulators. It will also be of paramount importance to extend our analysis of the C2 barrel column itself to include GABAergic neurons, which form the other major class of cortical neurons. Finally, it will also be necessary to study synaptic transmission in vivo (Crochet et al., 2005), which will introduce further complexity through interactions with spontaneous activity and different brain states.

Our quantification of the cortical excitatory microcircuit of the C2 barrel column in vitro is likely to provide an underestimate of the in vivo synaptic connectivity. Truncation of axons and dendrites in the slice preparation presumably reduces the number and amplitude of synaptic connections, particularly

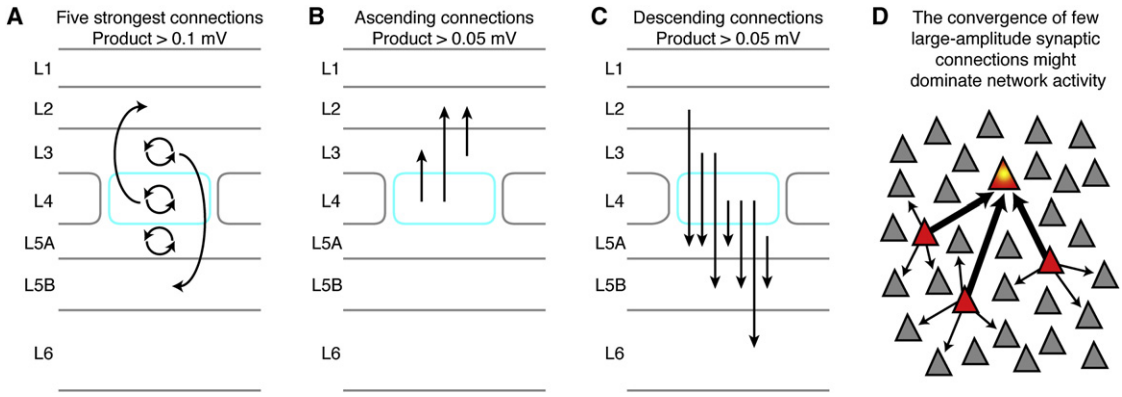

Figure 8. Schematic Summary

(A) The product of the probability of finding a given layer-specific synaptic connection and its mean uEPSP amplitude was used to evaluate the efficacy of the layer-specific excitatory pathways. Thresholding this product at a value of 0.1 mV revealed the five strongest connections, which are schematically drawn: L4→L2, L3→L3, L4→L4, L5A→L5A, and L3→L5B.

(B) Schematic drawing of the three strongest upward-oriented projections (thresholded at a product value of 0.05 mV): L4→L3, L4→L2, and L3→L2.

(C) Schematic drawing of the seven strongest downward-oriented projections (thresholded at a product value of 0.05 mV): L2→L5A, L3→L5A, L3→L5B, L4→L5A, L4→L5B, L4→L6, and L5A→L5B.

(D) Activity within networks with sparse AP firing may predominantly be mediated by the convergence of few large-amplitude synaptic inputs. Three spiking neurons (colored red) are schematically shown to evoke large-amplitude synaptic input (thick arrows) converging onto a single postsynaptic neuron that in turn is driven to fire an AP. The many unreliable small-amplitude synaptic connections (small arrows) may contribute little to network activity during sparse AP firing.

for distant cell pairs. These effects are reduced by recording from cells deep in the slice and orienting the plane of the slice to optimally include the C2 barrel column. In this context it is interesting to note that connectivity of some projections increases with distance, e.g., L5A connects more strongly to L2 than to the closer L3 and L4 ($P_{L5A\rightarrow L2}$ = 4.3%, $P_{L5A\rightarrow L3}$ = 2.2%, $P_{L5A\rightarrow L4}$ = 0.7%) and L3 connects more strongly to L5B than to the closer L4 or L5A ($P_{L3\rightarrow L5B}$ = 12.2%, $P_{L3\rightarrow L5A}$ = 5.7%, $P_{L3\rightarrow L4}$ = 2.4%). A further reason for underestimating the true synaptic connectivity might arise from an inability to identify small-amplitude synaptic connections because of strong dendritic filtering (Nevian et al., 2007; Williams and Stuart, 2002).

In addition to layer specificity studied here, previous reports have found evidence for specific patterns of synaptic connectivity between neurons in the same layer but with different long-range projections (Sawatari and Callaway, 2000; Kozloski et al., 2001; Le Bé et al., 2007). Distinct subnetworks of neurons within a cortical column (Yoshimura et al., 2005; Kampa et al., 2006) might be specialized for processing specific types of information. It will be of great interest to further subdivide the excitatory neurons of the mouse C2 barrel column, perhaps through gene expression patterns (Gong et al., 2003; Sugino et al., 2006; Nelson et al., 2006), and to examine any potential subnetworks, which might for example link neurons with the same direction preference for whisker deflections.

Our results must therefore be considered only as a beginning, and much more experimental data is required before we can assemble a realistic working model (Markram, 2006) of the mouse C2 barrel column, including how it dynamically processes sensory information, how it develops beyond P18–21 (the age range studied here), and how it changes through alterations in sensory experience (Allen et al., 2003; Bender et al., 2006; Cheetham et al., 2007; Clem et al., 2008; Feldman and Brecht, 2005; Finnerty et al., 1999; Fox, 2002; Heynen et al., 2003; Maffei et al., 2004; Shepherd et al., 2003; Takahashi et al., 2003). Fortunately, remarkable technical progress is being made toward large-scale, high-resolution analysis of synaptic circuits (Nikolenko et al., 2007; Nagel et al., 2003; Boyden et al., 2005; Arenkiel et al., 2007; Petreanu et al., 2007; Wang et al., 2007; Briggman and Denk, 2006; Wickersham et al., 2007).

In this study, we have applied the multiple simultaneous whole-cell recording technique, which although labor intense, is currently the only approach capable of delivering quantitative functional measures of synaptic connectivity at the level of individually identified presynaptic and postsynaptic neurons. The cellular resolution of our connectivity measurements revealed a prominent role for the small fraction of large-amplitude reliable synaptic connections throughout the microcircuits of the C2 mouse barrel column. These strong synaptic connections appear to provide a mechanistic basis for understanding the membrane potential dynamics recorded in awake, behaving mice (Crochet and Petersen, 2006; Poulet and Petersen, 2008), and may form a solid backbone for sensory processing linking specific subnetworks of neurons into dynamically regulated cell assemblies.

Our data provide a first-order cellular-resolution description of the excitatory microcircuit of the mouse C2 barrel column. Detailed cellular-level synaptic circuit analysis of neuronal networks underlying specific sensorimotor behaviors combined with highly specific genetic manipulations (Aronoff and Petersen, 2008; Luo et al., 2008) may lead to significant progress in our understanding of the synaptic mechanisms underlying sensory perception.

EXPERIMENTAL PROCEDURES

Animals and Surgery

All experiments were carried out in accordance with authorizations approved by the Swiss Federal Veterinary Office. Mice aged P18–21 of the C57BL6J strain were anesthetized with urethane (1.5 mg/g). Paw withdrawal reflexes were nearly absent and were repeatedly monitored to assess the level of anesthesia. A further 10% of the initial dose of urethane was injected if required. A subcutaneous dose of lidocaine (1%) was also administered above the skull to decrease pain during acute incision. A heating blanket maintained the rectally measured body temperature at 37°C. The skin overlying the somatosensory cortex was removed and the bone gently scraped to clean remaining membranes. The mouse was subsequently attached to a metal head holder.

Intrinsic Optical Imaging

The cortical surface of the brain was imaged through the intact skull covered with preheated (37°C) Ringers' solution and a glass coverslip. The blood vessel pattern was visualized using 530 nm LED illumination to enhance contrast. Functional imaging was performed under 630 nm LED illumination. Reflected light was collected with a Qicam CCD camera (Q-imaging) coupled to a stereomicroscope (Leica MZ9.5) at 1.6× magnification. Images of 800 × 800 pixels were acquired at 10 Hz covering a 3.8 × 3.8 mm field of view. Sensory stimuli consisted of 10 Hz piezo-driven deflection of the C2 whisker over 4 s. Data acquisition and sensory stimulation were controlled via an ITC-18 (InstruTech, Port Washington, NY) using custom routines written in IgorPro (Wavemetrics Inc, Lake Oswego, OR).

Preparation of Brain Slices

A small craniotomy (~300 μm diameter) centered over the C2 barrel column location was made and fluorescent dye (DiI or SR101) was applied to the brain for 1–2 min. The brain was subsequently removed and 300 μm parasagittal (35° away from vertical) brain slices were cut on a vibratome (Leica VT1000S, Germany) in a standard ice-cold artificial cerebrospinal fluid (ACSF; containing 125 mM NaCl, 2.5 mM KCl, 25 mM D-glucose, 25 mM $NaHCO_3$, 1.25 mM NaH_2PO_4, 2 mM $CaCl_2$, and 1 mM $MgCl_2$) or in a modified ACSF (Bureau et al., 2006) (containing 110 mM choline chloride, 25 mM $NaHCO_3$, 25 mM D-glucose, 11.6 mM sodium ascorbate, 7 mM $MgCl_2$, 3.1 mM sodium pyruvate, 2.5 mM KCl, 1.25 mM NaH_2PO_4, and 0.5 mM $CaCl_2$). Slices were then transferred to a chamber containing standard ACSF oxygenated with 95% O_2/5% CO_2 at 35°C for 15 min and subsequently maintained at room temperature for at least 30 min prior to use.

Whole-Cell Recordings

Excitatory neurons (pyramidal cells or spiny stellate cells, according to their morphology and laminar location) between 50–80 μm below the surface of the slice were visualized with a 20×/0.95NA WI objective, 4× postmagnification, under video microscopy (Olympus BX51WI, Switzerland) coupled with infrared gradient contrast. Simultaneous whole-cell patch-clamp recordings in current-clamp mode were acquired from the somata of up to six neurons with Multiclamp 700A amplifiers (Axon Instruments, Molecular Devices, Foster City, CA). Patch-pipettes with 5–7 MΩ resistance were used. The pipette intracellular solution contained 135 mM K-gluconate, 4 mM KCl, 4 mM Mg-ATP, 10 mM Na_2-phosphocreatine, 0.3 mM Na-GTP, and 10 mM HEPES (pH 7.3, 280 mOsm). Biocytin (3 mg/ml) was added to the intracellular solution. Electrophysiological data were low-pass Bessel filtered at 5–10 kHz and digitized at 20–40 kHz (ITC-18). Membrane potential measurements were not corrected for the liquid junction potential. All recordings were carried out at 35°C and the slices were continually superfused with ACSF oxygenated with 95% O_2/5% CO_2.

Custom-written routines in IgorPro were used to analyze electrophysiological data and statistics. Data analyses are presented as mean ± SEM (except where otherwise indicated). Mean traces were obtained by averaging 20 sweeps. Sweeps with artifacts around the stimulation time and depolarized traces were discarded before computing the averaged trace. The baseline was computed as an average across 5 ms before the current injection. The uEPSP amplitude was calculated as the difference between the mean voltage averaged across 1 ms at ±0.5 ms around the peak of the uEPSP and the previously computed baseline. The half-width is defined as the difference between the time when the voltage of the uEPSP reaches 50% of the amplitude in the rising phase and the time when 50% of the uEPSP amplitude is reached during the decay phase of the uEPSP. The rise time corresponds to the time on the rising phase from 20% to 80% of the uEPSP amplitude. The decay time was computed from a single exponential fit from 80% to 20% of the uEPSP amplitude on the falling phase. Prior to calculating the latency, a linear fit from 20% to 50% of the rising phase was performed. The time point corresponding to the back-extrapolated crossing of the linear fit with the baseline was taken as the starting point of the EPSP. The latency was then computed as the difference between the times when the presynaptic AP peaks and the uEPSP starting point. Time-to-peak corresponds to the difference between the uEPSP peak time point and uEPSP starting time point. The coefficient of variation (the standard deviation divided by the mean) of uEPSP amplitude was corrected for baseline noise by subtracting the variance of the baseline noise from the variance of the uEPSP amplitude. The baseline noise was computed in the same way as the amplitude of the uEPSP for four different time points before the presynaptic AP.

Statistical analyses were carried out in IgorPro (version 6.03). Statistically significant differences ($p < 0.05$) in Table 1, Table S1, and Table S3 were assessed by performing a nonparametric Kruskal-Wallis test followed by a post hoc Dunn-Holland-Wolfe test for pairwise comparison. Statistically significant differences ($p < 0.05$) in connectivity (in main text and Table 2 denoted as χ^2 test) were computed by a χ^2 statistic on contingency table with Bonferroni correction for multiple comparisons.

Anatomy

After completion of the electrophysiological recordings, slices were fixed for at least 24 hr in 4% paraformaldehyde and then transferred into phosphate buffer (PB, containing 0.1 M NaH_2PO_4 and 0.1 M Na_2HPO_4 [pH 7.3]). Slices were then washed in PB six times over a period of 2 hr. Endogenous peroxidases were quenched with 1% H_2O_2 in PB for 15 min. After another 2 hr of washing in PB, slices were conjugated with avidin-biotinylated peroxidase (ABC-Elite; Vector Laboratories) following the manufacturer's instructions. Slices were subsequently washed six times and biocytin was revealed using 0.5 mg/ml diaminobenzidine and 0.01% H_2O_2 in PB. The enzymatic reaction was monitored under visual control and stopped by washing with PB when the neuronal anatomy was clearly visible. Slices were then stained with 1 μM DAPI for 30 min and mounted on glass slides with mowiol. 3D neuronal reconstruction was performed under an upright microscope (Olympus BX51WI, Switzerland) through a 100×/1.4NA oil objective using Neurolucida (MicroBrightField Inc, USA).

For cell counts, the C2 barrel columns of GAD67-GFP knockin mice (Tamamaki et al., 2003) were labeled with injection of dextran-coupled Alexa 647 into the location mapped by intrinsic optical imaging. Subsequently, 100 μm thick parasagittal slices were cut using a vibratome (Leica VT1000S). Slices were washed in PB over 2 hr and incubated with a blocking medium containing 5% horse serum, 0.2% Triton X-100, and 1% BSA in PB for 1 hr. Slices were washed five times over 1 hr prior to overnight incubation with the neuron-specific biotinylated primary antibody (NeuN 1:100 in 0.1% Triton X-100, 5% horse serum; Chemicon). Slices were rinsed in PB for 1 hr and conjugated with an Alexa-594-coupled streptavidin (1:100; Molecular Probes Inc., Eugene, OR) in 0.1% Triton X-100 for 2 hr. Finally, slices were rinsed over 1 hr in PB and incubated in 1 μM DAPI prior to mounting on slides with Dabco. 3D confocal stacks (LEICA SP2 scanning confocal, 10×/0.4NA objective, Leica Microsystems, Switzerland) of the C2 barrel column were analyzed for six mice by an automated spot detection algorithm followed by manual correction and verification (IMARIS 6.1, Bitplane AG and Matlab 7.5, MathWorks SA).

Network Simulations

The NEST environment (Diesmann and Gewaltig, 2002) was used to simulate the neuronal network. An integrate-and-fire model with exponentially decaying postsynaptic currents was used (Gerstner and Kistler, 2002). The programming language Python was utilized to implement the network. The number of neurons in each layer of the model approximated the experimentally determined numbers of excitatory neurons: L2, 550; L3, 1150; L4, 1650; L5A, 450; L5B, 650; and L6, 1300. Resting membrane potential and AP threshold were

set according to the experimentally determined layer-specific means. Kinetics of uEPSPs were set to the experimentally determined layer-specific means and we assumed linear summation. The neuronal network was synaptically connected at the layer-specific experimentally observed probabilities by drawing randomly from the experimentally observed uEPSP amplitude distribution. We also tested two further networks wired with the same layer-specific connection probabilities except that (1) in one network the amplitude of each synaptic connection was replaced by its layer-specific mean and (2) in the other network all synaptic connections with a strength of less than 500 μV were eliminated. To test the threshold number of stimulated neurons necessary to generate further APs within the network, we performed multiple runs of the simulation. In each, a certain number of neurons were excited to see if further spikes could be observed. The number of excited neurons was increased with each run. The supracritical number of stimulated neurons necessary to produce a further spike was recorded as the threshold number for driving polysynaptic network activity. This procedure was repeated 26 times, each time with a different randomized pattern of neuronal network connectivity. We report the mean ± SD number of synchronously active neurons required for generating further APs in the network.

SUPPLEMENTAL DATA

The supplemental data for this article include three tables and six figures and can be found at http://www.neuron.org/supplemental/S0896-6273(08)01092-1.

ACKNOWLEDGMENTS

We thank Dirk Feldmeyer, Egbert Welker, and Wulfram Gerstner for useful discussions. We thank James Poulet and Luc Gentet for comments on the manuscript. We thank Luca Gambazzi for help with electronics; Rodrigo Perin and Raphael Holzer for help with IgorPro programming; Debasree Banerjee for help with reconstructions; and Alessandra Griffa for writing the Matlab image analysis tools for the manual verification of cell counts. We thank Kaspar Vogt for GAD67-GFP knockin mice, originally made by Yuchio Yanagawa. This work was supported by grants from the Swiss National Science Foundation and the European Union.

Accepted: December 4, 2008
Published: January 28, 2009

REFERENCES

Allen, C.B., Celikel, T., and Feldman, D.E. (2003). Long-term depression induced by sensory deprivation during cortical map plasticity in vivo. Nat. Neurosci. *6*, 291–299.

Arenkiel, B.R., Peca, J., Davison, I.G., Feliciano, C., Deisseroth, K., Augustine, G.J., Ehlers, M.D., and Feng, G. (2007). In vivo light-induced activation of neural circuitry in transgenic mice expressing channelrhodopsin-2. Neuron *54*, 205–218.

Aronoff, R., and Petersen, C.C.H. (2008). Layer, column and cell-type specific genetic manipulation in mouse barrel cortex. Front. Neurosci. *2*, 64–71.

Bender, K.J., Allen, C.B., Bender, V.A., and Feldman, D.E. (2006). Synaptic basis for whisker deprivation-induced synaptic depression in rat somatosensory cortex. J. Neurosci. *26*, 4155–4165.

Binzegger, T., Douglas, R.J., and Martin, K.A. (2004). A quantitative map of the circuit of cat primary visual cortex. J. Neurosci. *24*, 8441–8453.

Boyden, E.S., Zhang, F., Bamberg, E., Nagel, G., and Deisseroth, K. (2005). Millisecond-timescale, genetically targeted optical control of neural activity. Nat. Neurosci. *8*, 1263–1268.

Braitenberg, V., and Schüz, A. (1998). Cortex: Statistics and Geometry of Neuronal Connectivity (Berlin: Springer-Verlag).

Brasier, D.J., and Feldman, D.E. (2008). Synapse-specific expression of functional presynaptic NMDA receptors in rat somatosensory cortex. J. Neurosci. *28*, 2199–2211.

Brecht, M., Schneider, M., Sakmann, B., and Margrie, T.W. (2004). Whisker movements evoked by stimulation of single pyramidal cells in rat motor cortex. Nature *427*, 704–710.

Briggman, K.L., and Denk, W. (2006). Towards neural circuit reconstruction with volume electron microscopy techniques. Curr. Opin. Neurobiol. *16*, 562–570.

Brunel, N., Hakim, V., Isope, P., Nadal, J.P., and Barbour, B. (2004). Optimal information storage and the distribution of synaptic weights: perceptron versus Purkinje cell. Neuron *43*, 745–757.

Bureau, I., Shepherd, G.M., and Svoboda, K. (2004). Precise development of functional and anatomical columns in the neocortex. Neuron *42*, 789–801.

Bureau, I., von Saint Paul, F., and Svoboda, K. (2006). Interdigitated paralemniscal and lemniscal pathways in the mouse barrel cortex. PLoS Biol. *4*, e382.

Callaway, E.M., and Katz, L.C. (1993). Photostimulation using caged glutamate reveals functional circuitry in living brain slices. Proc. Natl. Acad. Sci. USA *90*, 7661–7665.

Cheetham, C.E., Hammond, M.S., Edwards, C.E., and Finnerty, G.T. (2007). Sensory experience alters cortical connectivity and synaptic function site specifically. J. Neurosci. *27*, 3456–3465.

Clem, R.L., Celikel, T., and Barth, A.L. (2008). Ongoing in vivo experience triggers synaptic metaplasticity in the neocortex. Science *319*, 101–104.

Crochet, S., and Petersen, C.C.H. (2006). Correlating whisker behavior with membrane potential in barrel cortex of awake mice. Nat. Neurosci. *9*, 608–610.

Crochet, S., Chauvette, S., Boucetta, S., and Timofeev, I. (2005). Modulation of synaptic transmission in neocortex by network activities. Eur. J. Neurosci. *21*, 1030–1044.

Diesmann, M., and Gewaltig, M.-O. (2002). NEST: An environment for neural systems simulations. In T. Plesser and V. Macho (Eds.), Forschung und wisschenschaftliches Rechnen, Beitrage zum Heinz-Billing-Preis 2001, Volume 58 of GWDG-Bericht, (pp. 43-70). Gottingen: Ges. fur Wiss. Datenverarbeitung.

Douglas, R.J., Koch, C., Mahowald, M., Martin, K.A.C., and Suarez, H.H. (1995). Recurrent excitation in neocortical circuits. Science *269*, 981–985.

Feldman, D.E. (2000). Timing-based LTP and LTD at vertical inputs to layer II/III pyramidal cells in rat barrel cortex. Neuron *27*, 45–56.

Feldman, D.E., and Brecht, M. (2005). Map plasticity in somatosensory cortex. Science *310*, 810–815.

Feldmeyer, D., Egger, V., Lübke, J., and Sakmann, B. (1999). Reliable synaptic connections between pairs of excitatory layer 4 neurones within a single 'barrel' of developing rat somatosensory cortex. J. Physiol. *521*, 169–190.

Feldmeyer, D., Lübke, J., Silver, R.A., and Sakmann, B. (2002). Synaptic connections between layer 4 spiny neurone-layer 2/3 pyramidal cell pairs in juvenile rat barrel cortex: physiology and anatomy of interlaminar signalling within a cortical column. J. Physiol. *538*, 803–822.

Feldmeyer, D., Roth, A., and Sakmann, B. (2005). Monosynaptic connections between pairs of spiny stellate cells in layer 4 and pyramidal cells in layer 5A indicate that lemniscal and paralemniscal afferent pathways converge in the infragranular somatosensory cortex. J. Neurosci. *25*, 3423–3431.

Feldmeyer, D., Lübke, J., and Sakmann, B. (2006). Efficacy and connectivity of intracolumnar pairs of layer 2/3 pyramidal cells in the barrel cortex of juvenile rats. J. Physiol. *575*, 583–602.

Ferezou, I., Bolea, S., and Petersen, C.C.H. (2006). Visualizing the cortical representation of whisker touch: voltage-sensitive dye imaging in freely moving mice. Neuron *50*, 617–629.

Ferezou, I., Haiss, F., Gentet, L.J., Aronoff, R., Weber, B., and Petersen, C.C.H. (2007). Spatiotemporal dynamics of cortical sensorimotor integration in behaving mice. Neuron *56*, 907–923.

Finnerty, G.T., Roberts, L.S., and Connors, B.W. (1999). Sensory experience modifies the short-term dynamics of neocortical synapses. Nature *400*, 367–371.

Fox, K. (2002). Anatomical pathways and molecular mechanisms for plasticity in the barrel cortex. Neuroscience *111*, 799–814.

Frick, A., Feldmeyer, D., Helmstaedter, M., and Sakmann, B. (2008). Monosynaptic connections between pairs of L5A pyramidal neurons in columns of juvenile rat somatosensory cortex. Cereb. Cortex *18*, 397–406.

Gerstner, W., and Kistler, W. (2002). Spiking Neuron Models: Single Neurons, Populations, Plasticity (United Kingdom: Cambridge University Press).

Gilbert, C.D., and Sigman, M. (2007). Brain states: top-down influences in sensory processing. Neuron *54*, 677–696.

Gong, S., Zheng, C., Doughty, M.L., Losos, K., Didkovsky, N., Schambra, U.B., Nowak, N.J., Joyner, A., Leblanc, G., Hatten, M.E., and Heintz, N. (2003). A gene expression atlas of the central nervous system based on bacterial artificial chromosomes. Nature *425*, 917–925.

Greenberg, D.S., Houweling, A.R., and Kerr, J.N. (2008). Population imaging of ongoing neuronal activity in the visual cortex of awake rats. Nat. Neurosci. *11*, 749–751.

Grinvald, A., Lieke, E., Frostig, R.D., Gilbert, C.D., and Wiesel, T.N. (1986). Functional architecture of cortex revealed by optical imaging of intrinsic signals. Nature *324*, 361–364.

Harris, J.A., Petersen, R.S., and Diamond, M.E. (1999). Distribution of tactile learning and its neural basis. Proc. Natl. Acad. Sci. USA *96*, 7587–7591.

Hebb, D.O. (1949). The Organization of Behaviour (New York: Wiley).

Heynen, A.J., Yoon, B.J., Liu, C.H., Chung, H.J., Huganir, R.L., and Bear, M.F. (2003). Molecular mechanism for loss of visual cortical responsiveness following brief monocular deprivation. Nat. Neurosci. *6*, 854–862.

Houweling, A.R., and Brecht, M. (2008). Behavioural report of single neuron stimulation in somatosensory cortex. Nature *451*, 65–68.

Huber, D., Petreanu, L., Ghitani, N., Ranade, S., Hromádka, T., Mainen, Z., and Svoboda, K. (2008). Sparse optical microstimulation in barrel cortex drives learned behaviour in freely moving mice. Nature *451*, 61–64.

Hutson, K.A., and Masterton, R.B. (1986). The sensory contribution of a single vibrissa's cortical barrel. J. Neurophysiol. *56*, 1196–1223.

Kampa, B.M., Letzkus, J.J., and Stuart, G.J. (2006). Cortical feed-forward networks for binding different streams of sensory information. Nat. Neurosci. *9*, 1472–1473.

Kozloski, J., Hamzei-Sichani, F., and Yuste, R. (2001). Stereotyped position of local synaptic targets in neocortex. Science *293*, 868–872.

Le Bé, J.V., Silberberg, G., Wang, Y., and Markram, H. (2007). Morphological, electrophysiological, and synaptic properties of corticocallosal pyramidal cells in the neonatal rat neocortex. Cereb. Cortex *17*, 2204–2213.

Lee, A.K., Manns, I.D., Sakmann, B., and Brecht, M. (2006). Whole-cell recordings in freely moving rats. Neuron *51*, 399–407.

Luo, L., Callaway, E.M., and Svoboda, K. (2008). Genetic dissection of neural circuits. Neuron *57*, 634–660.

Maffei, A., Nelson, S.B., and Turrigiano, G.G. (2004). Selective reconfiguration of layer 4 visual cortical circuitry by visual deprivation. Nat. Neurosci. *7*, 1353–1359.

Markram, H. (2006). The blue brain project. Nat. Rev. Neurosci. *7*, 153–160.

Markram, H., Lübke, J., Frotscher, M., and Sakmann, B. (1997). Regulation of synaptic efficacy by coincidence of postsynaptic APs and EPSPs. Science *275*, 213–215.

Nagel, G., Szellas, T., Huhn, W., Kateriya, S., Adeishvili, N., Berthold, P., Ollig, D., Hegemann, P., and Bamberg, E. (2003). Channelrhodopsin-2, a directly light-gated cation-selective membrane channel. Proc. Natl. Acad. Sci. USA *100*, 13940–13945.

Nelson, S.B., Sugino, K., and Hempel, C.M. (2006). The problem of neuronal cell types: a physiological genomics approach. Trends Neurosci. *29*, 339–345.

Nevian, T., Larkum, M.E., Polsky, A., and Schiller, J. (2007). Properties of basal dendrites of layer 5 pyramidal neurons: a direct patch-clamp recording study. Nat. Neurosci. *10*, 206–214.

Nikolenko, V., Poskanzer, K.E., and Yuste, R. (2007). Two-photon photostimulation and imaging of neural circuits. Nat. Methods *4*, 943–950.

Petersen, C.C.H. (2007). The functional organization of the barrel cortex. Neuron *56*, 339–355.

Petersen, C.C.H., and Sakmann, B. (2000). The excitatory neuronal network of rat layer 4 barrel cortex. J. Neurosci. *20*, 7579–7586.

Petersen, C.C.H., and Sakmann, B. (2001). Functionally independent columns of rat somatosensory barrel cortex revealed with voltage-sensitive dye imaging. J. Neurosci. *21*, 8435–8446.

Petreanu, L., Huber, D., Sobczyk, A., and Svoboda, K. (2007). Channelrhodopsin-2-assisted circuit mapping of long-range callosal projections. Nat. Neurosci. *10*, 663–668.

Poulet, J.F.A., and Petersen, C.C.H. (2008). Internal brain state regulates membrane potential synchrony in barrel cortex of behaving mice. Nature *454*, 881–885.

Sarid, L., Bruno, R., Sakmann, B., Segev, I., and Feldmeyer, D. (2007). Modeling a layer 4-to-layer 2/3 module of a single column in rat neocortex: interweaving in vitro and in vivo experimental observations. Proc. Natl. Acad. Sci. USA *104*, 16353–16358.

Sawatari, A., and Callaway, E.M. (2000). Diversity and cell type specificity of local excitatory connections to neurons in layer 3B of monkey primary visual cortex. Neuron *25*, 459–471.

Schubert, D., Staiger, J.F., Cho, N., Kötter, R., Zilles, K., and Luhmann, H.J. (2001). Layer-specific intracolumnar and transcolumnar functional connectivity of layer V pyramidal cells in rat barrel cortex. J. Neurosci. *21*, 3580–3592.

Schubert, D., Kötter, R., Zilles, K., Luhmann, H.J., and Staiger, J.F. (2003). Cell type-specific circuits of cortical layer IV spiny neurons. J. Neurosci. *23*, 2961–2970.

Schubert, D., Kötter, R., Luhmann, H.J., and Staiger, J.F. (2006). Morphology, electrophysiology and functional input connectivity of pyramidal neurons characterizes a genuine layer Va in the primary somatosensory cortex. Cereb. Cortex *16*, 223–236.

Shepherd, G.M., and Svoboda, K. (2005). Laminar and columnar organization of ascending excitatory projections to layer 2/3 pyramidal neurons in rat barrel cortex. J. Neurosci. *25*, 5670–5679.

Shepherd, G.M., Pologruto, T.A., and Svoboda, K. (2003). Circuit analysis of experience-dependent plasticity in the developing rat barrel cortex. Neuron *38*, 277–289.

Shepherd, G.M., Stepanyants, A., Bureau, I., Chklovskii, D., and Svoboda, K. (2005). Geometric and functional organization of cortical circuits. Nat. Neurosci. *8*, 782–790.

Silberberg, G., Grillner, S., LeBeau, F.E., Maex, R., and Markram, H. (2005). Synaptic pathways in neural microcircuits. Trends Neurosci. *28*, 541–551.

Silver, R.A., Lubke, J., Sakmann, B., and Feldmeyer, D. (2003). High-probability uniquantal transmission at excitatory synapses in barrel cortex. Science *302*, 1981–1984.

Sjöström, P.J., Turrigiano, G.G., and Nelson, S.B. (2001). Rate, timing, and cooperativity jointly determine cortical synaptic plasticity. Neuron *32*, 1149–1164.

Sjöström, P.J., Turrigiano, G.G., and Nelson, S.B. (2003). Neocortical LTD via coincident activation of presynaptic NMDA and cannabinoid receptors. Neuron *39*, 641–654.

Song, S., Sjöström, P.J., Reigl, M., Nelson, S.B., and Chklovskii, D.B. (2005). Highly nonrandom features of synaptic connectivity in local cortical circuits. PLoS Biol. *3*, e68.

Sugino, K., Hempel, C.M., Miller, M.N., Hattox, A.M., Shapiro, P., Wu, C., Huang, Z.J., and Nelson, S.B. (2006). Molecular taxonomy of major neuronal classes in the adult mouse forebrain. Nat. Neurosci. *9*, 99–107.

Takahashi, T., Svoboda, K., and Malinow, R. (2003). Experience strengthening transmission by driving AMPA receptors into synapses. Science *299*, 1585–1588.

Tamamaki, N., Yanagawa, Y., Tomioka, R., Miyazaki, J., Obata, K., and Kaneko, T. (2003). Green fluorescent protein expression and colocalization with calretinin, parvalbumin, and somatostatin in the GAD67-GFP knock-in mouse. J. Comp. Neurol. *467*, 60–79.

Thomson, A.M., and Lamy, C. (2007). Functional maps of neocortical local circuitry. Front. Neurosci. *1*, 19–42.

Wang, H., Peca, J., Matsuzaki, M., Matsuzaki, K., Noguchi, J., Qiu, L., Wang, D., Zhang, F., Boyden, E., Deisseroth, K., et al. (2007). High-speed mapping of synaptic connectivity using photostimulation in Channelrhodopsin-2 transgenic mice. Proc. Natl. Acad. Sci. USA *104*, 8143–8148.

Watts, D.J., and Strogatz, S.H. (1998). Collective dynamics of 'small-world' networks. Nature *393*, 440–442.

Weiler, N., Wood, L., Yu, J., Solla, S.A., and Shepherd, G.M. (2008). Top-down laminar organization of the excitatory network in motor cortex. Nat. Neurosci. *11*, 360–366.

Wickersham, I.R., Lyon, D.C., Barnard, R.J., Mori, T., Finke, S., Conzelmann, K.K., Young, J.A., and Callaway, E.M. (2007). Monosynaptic restriction of transsynaptic tracing from single, genetically targeted neurons. Neuron *53*, 639–647.

Williams, S.R., and Stuart, G.J. (2002). Dependence of EPSP efficacy on synapse location in neocortical pyramidal neurons. Science *295*, 1907–1910.

Woolsey, T.A., and Van der Loos, H. (1970). The structural organization of layer IV in the somatosensory region (SI) of mouse cerebral cortex. The description of a cortical field composed of discrete cytoarchitectonic units. Brain Res. *17*, 205–242.

Yoshimura, Y., Dantzker, J.L., and Callaway, E.M. (2005). Excitatory cortical neurons form fine-scale functional networks. Nature *433*, 868–873.